TWENTYFIFTH EUROPEAN ROTORCRAFT FORUM

Paper No. N6

AN INVESTIGATION OF THE AEROELASTIC STABILITY OF A HELICOPTER BLADE WITH A "SMART" SPRING AT THE ROOT

BY

S. SOLAIMAN, RESEARCH ASSISTANT,
CARLETON UNIVERSITY
OTTAWA, ON, K1S 5B6, CANADA

F. F. AFAGH, PROFESSOR,
CARLETON UNIVERSITY
OTTAWA, ON, K1S 5B6, CANADA

F. NITZSCHE, SENIOR RESEARCH OFFICER,
NATIONAL RESEARCH COUNCIL CANADA /
INSTITUTE FOR AEROSPACE RESEARCH
OTTAWA, ON, K1A 0R6, CANADA

SEPTEMBER 14-16, 1999
ROME, ITALY

ASSOCIAZIONE INDUSTRIE PER L'AEROSPAZIO, I SISTEMI E LA DIFESA
ASSOCIAZIONE ITALIANA SI AERONAUTICA ED ASTRONAUTICA

An Investigation of the Aeroelastic Stability of a Helicopter Blade with a "Smart" Spring at the Root

S. Solaiman, Research Assistant,
Carleton University,
Ottawa, ON, K1S 5B6, Canada

Fred F. Afagh, Professor,
Carleton University,
Ottawa, ON, K1S 5B6, Canada

Fred Nitzsche, Senior Research Officer,
National Research Council Canada / Institute for Aerospace Research
Ottawa, ON, K1A 0R6, Canada

In the present study, the three-dimensional, non-linear, aeroelastic stability of a helicopter rotor blade when subjected to harmonic parametric excitation is investigated. The analysis is conducted using Floquet's theory for the stability of periodic systems. Using a square-wave (on-off) control law with frequencies of 3, 4 and 5/rev, the stability margins of a "smart" hingeless blade incorporating a harmonic parametric excitation device under development at the National Research Council of Canada are obtained for the hover condition and compared with a baseline case. The results indicate that the stability of the periodic system is greatly enhanced when the actuation is performed. The analysis demonstrates that significant shifts in the modal frequencies as well as the damping of the system result from actuation, suggesting the feasibility of tailoring the forced frequency response of the blade with such a device.

a	Lift-curve slope
A	Section area, $\iint_A d\eta d\zeta$
B	Number of blades
c	Blade chord
c_{d_0}	Drag coefficient
E	Young's modulus
G	Shear modulus
$I_{y'}, I_{z'}$	Area moments of inertia, $\iint_A \zeta^2 d\eta d\zeta, \iint_A \eta^2 d\eta d\zeta$
J	Area polar moment of inertia corrected for warping, $\iint_A (\hat{\eta}^2 + \hat{\zeta}^2) d\eta d\zeta$
${k_A}^2$	Area radius of gyration, $\iint_A (\eta^2 + \zeta^2) d\eta d\zeta / A$
${k_m}^2$	Mass radius of gyration, ${k_{m_1}}^2 + {k_{m_2}}^2$
${k_{m_1}}^2, {k_{m_2}}^2$	$\iint_A \rho \zeta^2 \, d\eta d\zeta / m$, $\iint_A \rho \eta^2 \, d\eta d\zeta / m$
L_v, L_w	Aerodynamic forces in the v- and w-directions per unit of length
m	Mass per unit of length, $\iint_A \rho d\eta d\zeta$
$\overline{m}_{ss}$	Mass per unit of length due to "smart" spring
M,C,K	Generalized mass, damping and stiffness matrices
$\Delta M, \Delta C, \Delta K$	Generalized mass, damping and stiffness matrices due to "smart" spring
M_ϕ	Aerodynamic moment in the ϕ-direction per unit of length

P,Q	Matrix of periodic coefficients, transition matrix solution
R	Rotor radius
t	Time
T	Period of actuation
u, v, w	Blade extensional, lead-lag and flap bending displacements (along x, y, z)
U	Matrix of non-rotating eigenvectors
v_i	Rotor induced velocity
x, y, z	Undeformed blade coordinate system (x is the elastic axis)
X	Vector of generalized perturbations
β_{pc}	Pre-cone angle
γ	Lock number, $3\rho_\infty acR/m$
η, ζ	Principle coordinate system of the blade cross section
θ	Blade pitch angle
κ_{ss}	Dimensionless torsional rigidity due to "smart" spring
λ	Eigenvalues of the transition matrix
$\Lambda_{1ss}, \Lambda_{2ss}$	Dimensionless bending stiffnesses due to "smart" spring
$\mu_{ss}, \mu_{1ss}, \mu_{2ss}$	Dimensionless radii of gyration due to "smart" spring
ρ, ρ_∞	Structural mass density, air density
σ	Rotor solidity, $Bc/\pi R$
ϕ, ϕ_0	Torsional displacement, torsional displacement at steady-state (trim) condition
ψ	Azimuth angle
ω, ξ	Frequency, damping of the aeroelastic mode
ω^2_{NR}	Matrix of non-rotating eigenvalues squared
Ω	Rotor spin velocity
$(\ )'$	Derivative with respect to x
$(\dot{\ })$	Derivative with respect to t or ψ
$(\bar{\ })$	Non-dimensionalized quantity
Subscript ss	Refers to "smart" spring

1.0. Introduction and Background

Presently, two types of helicopter rotor configurations are manufactured by the rotorcraft industry. The hingeless blade, in which the flap and lead-lag hinges are absent, and the more mechanically complex configuration of the articulated blade with the flap and lead-lag hinges. The hingeless configuration is of particular interest due to the fact that it affords an increased controllability. However, due to the nature of its configuration, a hingeless rotor can be easily susceptible to instability problem. This problem is caused by the non-linear coupling that occurs between the flap, lead-lag and torsional motions of the cantilever blade. The strong coupling of these motions make the analysis of the hingeless rotor a complicated and important subject.

This paper presents the results of a study to develop and simulate the behaviour of a "smart-hingeless helicopter blade". The spectrum of loads associated with the non-homogeneous forcing loads was tuned by superimposing a harmonic system on the rotating frame. The Individual Blade Control (IBC) concept pioneered by Kretz (Ref. 1) and Ham (Ref. 2) was used in this approach. The IBC allows the control of a broad range of frequencies by using actuators installed either on the helicopter swashplate or individually attached on the blades. In this way, using a number of control subsystems, one may control a number of modes of vibration introduced during the operation of the aircraft. The IBC method is very appropriate for situations in which each blade has its own characteristics. By synthesizing a suitable control system on an individual blade, the modes of vibration occurring on that particular blade can be minimized leading to reduced loads transferred to the helicopter airframe.

Two strategies are available in connection with the use of the IBC approach. The first one involves the use of embedded adaptive materials in the composite construction of the helicopter blade. This is intended to induce strain deformations, which are controlled externally. The strategy allows the possibility of achieving special features of the application of distributed control theory, such as superior robustness. In addition, it has the advantage of being smoother from the aerodynamic point of view. However, several studies have shown that this strategy overestimates the capability of the adaptive materials to induce the necessary strain deformations under typical helicopter operational loads. This leads to the utilization of the second strategy, namely the lumped parameter control approach which was initiated by Spangler and Hall (Ref. 3). This approach is based on the idea of controlling some segment of a helicopter blade using smart actuators. To date, the most accepted solution using this approach has been the use of a "smart flap" by installing adaptive

actuators at the flaps on the trailing edge of the helicopter blade. Another idea has been to use adaptive actuators to deform the airfoil shape to actively control rotary wing characteristics such as: dynamic stall, blade vortex interaction and shock. However, an interesting alternative, on which this paper is based on, was introduced by Nitzsche, Lammering and Breitbach (Ref. 4). According to this concept, by actuating the "smart" spring, an Individual Blade Control device developed at the National Research Council of Canada, implemented at the blade root, one may alter the aeroelastic stability of the rotor.

2.0. Governing Differential of the Main Rotor

The main objective of this study is to investigate the aeroelastic stability of the rotating blade system undergoing parametric harmonic excitation using the "smart" spring that modifies the impedance of the blade structure (Ref. 5). As an initial attempt only hover flight conditions are considered. Moreover, the main rotor is modeled as a uniform, long, straight, slender, homogeneous isotropic beam with a constant axial twist for which the offsets between the tension, elastic, mass and aerodynamic axes are negligible.

Using two complimentary methods: (1) the variational method based on Hamilton's principle, and (2) the Newtonian method, Hodges and Dowell derived the non-linear flap-lag-torsion equations of motion of a twisted non-uniform rotor (Ref. 6). Later, Hodges and Ormiston simplified these equations for a uniform rotor blade and investigated the associated stability problem (Ref. 7). These simplifications reflect the fact that no chord-wise offsets are assumed to be present between the elastic, mass, tension, and aerodynamic centers on the blade cross section. Moreover, the unloaded blade has no pre-twist along the axial direction. The main parameters influencing the stability were found to be the structural coupling between the flap and lag bending as well as the torsion stiffness.

The blade elastic displacements considered are the axial u, the lead-lag bending v, and the flap bending w, and the twist ϕ (Figure 1). In the derivation of the equations of motion, an ordering scheme based on the restriction that the squares of the bending slopes, torsion deformation, chord/radius and thickness/radius ratios were small compared to unity was adopted according to Hodges and Dowell (Ref. 6). Finally, the model can be simplified by solving for u in terms of the local tension, and assuming that the radial displacement of the rotor blade is a purely geometric consequence of the transverse bending deflections of the blade.

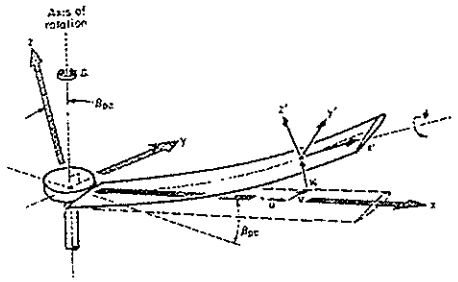

Figure 1: Blade definitions (Ref. 17).

It should be noted that such an assumption is valid only for sufficiently large values of dimensionless radial stiffness.

The following three equations for v, w, and ϕ can be derived (Ref. 7):

$$
\begin{aligned}
&-\frac{m\Omega^2}{2}\left[v'\left(R^2-x^2\right)\right]'-2m\Omega\left(v'\int_x^R \dot{v}dx\right)' \\
&+\left[EI_z-\left(EI_z-EI_y\right)\sin^2(\Re\theta)\right]v'''' \\
&+\left(EI_z-EI_y\right)\frac{\sin(2\Re\theta)}{2}w'''' \\
&+\left(EI_z-EI_y\right)\left[-\sin(2\Re\theta)(\phi v'')'+\cos(2\Re\theta)(\phi w'')'\right] \\
&-2m\Omega\beta_{pc}\dot{w}-2m\Omega\int_0^x(v'\dot{v}'+w'\dot{w}')dx+m\left(\ddot{v}-\Omega^2 v\right)=L_v
\end{aligned}
\tag{1}
$$

$$
\begin{aligned}
&-\frac{m\Omega^2}{2}\left[w'\left(R^2-x^2\right)\right]'-2m\Omega\left(w'\int_x^R \dot{v}dx\right)' \\
&+\left[EI_y+\left(EI_z-EI_y\right)\sin^2(\Re\theta)\right]w'''' \\
&+\left(EI_z-EI_y\right)\frac{\sin(2\Re\theta)}{2}v'''' \\
&+\left(EI_z-EI_y\right)\left[\cos(2\Re\theta)(\phi v'')'+\sin(2\Re\theta)(\phi w'')'\right] \\
&+2m\Omega\beta_{pc}\dot{v}+m\ddot{w}=L_w-m\Omega^2\beta_{pc}x
\end{aligned}
\tag{2}
$$

$$
\begin{aligned}
&-\frac{m\Omega^2}{2}k_A^{\,2}\left[\phi'\left(R^2-x^2\right)\right]'-GJ\phi''+mk_m^{\,2}\ddot{\phi} \\
&+m\Omega^2(k_{m_2}^{\,2}-k_{m_1}^{\,2})\phi\cos(2\theta) \\
&+\left(EI_z-EI_y\right)\left[\left(w''^2-v''^2\right)\frac{\sin(2\Re\theta)}{2}+v''w''\cos(2\Re\theta)\right] \\
&=M_\phi-m\Omega^2(k_{m_2}^{\,2}-k_{m_1}^{\,2})\frac{\sin(2\theta)}{2}
\end{aligned}
\tag{3}
$$

where $\Re$ is a flap-lag structural coupling parameter that can be assigned any arbitrary value between 0 to 1. This is an approximate representation of the fact that such a structural coupling is dependant on the relative stiffness of the blade segments in-board and out-board of the pitch bearing.

The aerodynamic loads applied to the rotor blade used in this study are based on Greenberg's extension of the Theodorsen's theory (Ref. 8). This model is valid for a two-dimensional airfoil undergoing sinusoidal motion in pulsating incompressible flow. The basis of this formulation is strip theory in which only velocity components in the directions perpendicular to the spanwise axis of the blade influence the aerodynamic loads. A quasi-steady approximation of the unsteady theory for low reduced frequencies is employed, in which the Theodorsen lift-deficiency function is taken to be unity. The classical blade element momentum theory is used to calculate the steady inflow for the rotor. The aerodynamic loads are, thus, expressed as:

$$L_v \cong \frac{\rho_\infty ac}{2}\{v_i^2 - \Omega^2 x^2 \frac{c_{d0}}{a} - \Omega x v_i(\theta+\phi) - \left[2\Omega x \frac{c_{d0}}{a} + (\theta+\phi)v_i\right]\dot{v} + \left[2v_i - \Omega x(\theta+\phi)\right]\dot{w}\} \tag{4}$$

$$L_w \cong \frac{\rho_\infty ac}{2}\{-\Omega x v_i + \Omega^2 x^2\left(\theta+\phi+\int_0^x v'w''dx\right) - \Omega^2 x v\left(\beta_{pc}+w'\right) + \Omega^2 \frac{xc}{2}\left(\beta_{pc}+w'\right) + \left[2\Omega x(\theta+\phi) - v_i\right]\dot{v} - \Omega x\dot{w} + \frac{3xc}{4}\Omega\dot{\phi} - \frac{c}{4}\ddot{w}\} \tag{5}$$

$$M_\phi \cong -\frac{\rho_\infty ac}{2}\left(\frac{xc^2}{8}\Omega\dot{\phi}\right) \tag{6}$$

where v_i is the induced inflow velocity that is taken to be steady and uniform along the blade radius and equal to the value of the non-uniform inflow given by blade momentum theory at 0.75 radius. The value of the blade angle at that particular position is equal to the pitch angle plus the equilibrium elastic twist at 0.75 radius. Thus:

$$v_i = \mathrm{sgn}\left[\theta+\phi_o(0.75R)\right]\Omega R\frac{\pi\sigma}{8}\left(\sqrt{1+\frac{12}{\pi\sigma}\left|\theta+\phi_o(0.75R)\right|}-1\right) \tag{7}$$

The non-linear, equations of motion with variable coefficients (Eqs. 1-3) are solved by Galerkin's method. To this end, once these equations are appropriately non-dimensionalized, in order to apply Galerkin's method, the flap, lead-lag and twist displacements are prescribed as a series in generalized coordinates and mode shape functions:

$$\bar{v} = \sum_{j=1}^{N} V_j(\psi)\Psi_j(\bar{x}), \quad \bar{w} = \sum_{j=1}^{N} W_j(\psi)\Psi_j(\bar{x}), \quad \phi = \sum_{j=1}^{N} \Phi_j(\psi)\Theta_j(\bar{x}) \tag{8}$$

where the non-dimensional quantities defined in Eq. 8 are:

$$\psi = \Omega t, \quad \bar{x} = \frac{x}{R}, \quad \bar{v} = \frac{v}{R}, \quad \bar{w} = \frac{w}{R} \tag{9}$$

The assumed comparison functions,

$$\Psi_j(\bar{x}) = \cosh(\beta_j\bar{x}) - \cos(\beta_j\bar{x}) - \alpha_j\left[\sinh(\beta_j\bar{x}) - \sin(\beta_j\bar{x})\right], \quad \Theta_j(\bar{x}) = \sqrt{2}\sin(\gamma_j\bar{x}) \tag{10}$$

are the non-rotating, uncoupled natural modes of a uniform cantilevered beam for which the constants α_j, β_j, and γ_j are tabulated (Ref. 9). Substituting Eq. 8 into Eqs. 1-6, and considering the expressions shown in Eq. 10, yields $3N$ equations of motion in terms of the generalized coordinates V_j, W_j, and ϕ_j, where N is the number of natural modes of the uniform beam retained. The resulting non-linear ordinary differential equations of motion are linearized for small perturbations about an equilibrium or trim condition. To achieve this, the generalized coordinates were decomposed into steady-state equilibrium quantities and small perturbations as follows:

$$V_j(\psi) = V_{oj} + \Delta V_j(\psi), \quad W_j(\psi) = W_{oj} + \Delta W_j(\psi), \quad \Phi_j(\psi) = \Phi_{oj} + \Delta\Phi_j(\psi) \tag{11}$$

This procedure led to two sets of equations of motion. By substituting the steady-state equilibrium quantities of the generalized displacements into the non-linear equations of motion, a first set of non-linear algebraic equilibrium equations was obtained. The second set of equations was available by substituting both the steady state and perturbation quantities of the generalized displacements into the original equations, subtracting the equilibrium equations

obtained above, and neglecting all the non-linear products of the perturbation quantities. A set of $3N$ linear differential equations on the perturbation quantities for which the coefficients were functions of the equilibrium solution was obtained. The latter equations define the blade perturbations about the equilibrium or trim displacements:

$$[M]\{\ddot{X}\}+[C]\{\dot{X}\}+[K]\{X\}=\{0\} \tag{12}$$

where the matrices are defined by Hodges and Ormiston (Ref. 17).

It is desirable to reduce the order of the system by transformation to modal coordinates. The real-valued, free-vibration eigenvalue problem associated with the non-rotating blade was solved:

$$[M_s][U][\omega_{NR}^2]=[K_s][U] \tag{13}$$

where the subscript s is applied to the corresponding matrices without the aerodynamic contribution. Hence the stability of the perturbed motion about the equilibrium condition is determined by the eigenvalues of the square matrix of dimension $2m$:

$$\begin{Bmatrix}\dot{\tilde{X}}\\ \ddot{\tilde{X}}\end{Bmatrix}=\begin{bmatrix}0 & I\\ -\tilde{M}^{-1}U^TKU & -\tilde{M}^{-1}U^TCU\end{bmatrix}\begin{Bmatrix}\tilde{X}\\ \dot{\tilde{X}}\end{Bmatrix} \tag{14}$$

where m is the number of modes retained and $\tilde{M}$ is the diagonal matrix:

$$[U]^T[M][U]=[\tilde{M}] \tag{15}$$

Another consequence of coordinate transformation $X=U\tilde{X}$ is that only the eigenvectors of the modal matrix U that correspond to the desired frequencies can be selected. For the present study, N=6 and m=4 (including the first lead-lag, first and second flap, and first torsion eigenvectors) were used. The aerodynamic terms in the mass matrix known as the apparent mass were of a smaller order of magnitude and thus neglected in the present analysis, i.e. $M \approx M_s$.

3.0. Hingeless Helicopter Rotors as "Smart" Structures

As it was noted earlier, due to the nature of its configuration, the hingeless blade can be susceptible to instability problem. This problem is caused by the non-linear coupling that occurs between the flap, lead-lag and torsional motions of the cantilever blade. To improve on the aeroelastic stability of the blade it is suggested that "smart" materials are introduced at desired locations along the blade. When actuated such a "smart" material will act as a "smart" spring affecting the cross sectional characteristics of the blade. The introduction and harmonic actuation of the "smart" materials necessitates a proper modification of the equations of motion developed by Hodges and Dowell (Ref. 6) in order to model a "smart" blade. This is accomplished by defining the flap, lag, and torsion stiffnesses as well as the radii of gyrations of the blade cross section as functions of the distance from the hub along the blade. Next, these functions are incorporated in the application of the Galerkin method to obtain the root loci of the perturbation equations, which are used to investigate the stability of the system.

3.1. Governing Differential of the "Smart" Rotor

The harmonic actuation of the "smart" spring that can be interpreted as a harmonic parametric excitation introduces a periodic change in the matrices defined in Eq. 12. A variation in the amplitude of these matrices, according to a square-wave form, will be added, representing actuation and de-actuation of the IBC system in an on-off configuration. Over one normalized period of the blade rotation, 2π, it will be assumed that the control system is activated at a frequency of n/rev. Hence, for a controlled blade the equations that define the blade perturbations about the trim displacements are:

$$\begin{aligned}&([M]+[\Delta M])\{\ddot{X}\}+([C]+[\Delta C])\{\dot{X}\}\\ &+([K]+[\Delta K])\{X\}=\{0\}\end{aligned} \tag{16}$$

where the new additional matrices due to the harmonic parametric actuation of the "smart" spring are defined by Solaiman and Afagh (Ref. 10) as:

$$[\Delta M]=\begin{bmatrix} \overline{m}_{ss}\delta_{sj1} & 0 & 0 \\ 0 & \overline{m}_{ss}\delta_{sj1} & 0 \\ 0 & 0 & \mu_{ss}^{\ 2}\delta_{sj2} \end{bmatrix}, \tag{17}$$

$$[\Delta C]=\begin{bmatrix} \Delta C_{11} & \Delta C_{12} & \Delta C_{13} \\ \Delta C_{21} & \Delta C_{22} & \Delta C_{23} \\ \Delta C_{31} & \Delta C_{32} & \Delta C_{33} \end{bmatrix}, \tag{18}$$

$$[\Delta K]=\begin{bmatrix} \Delta K_{11} & \Delta K_{12} & \Delta K_{13} \\ \Delta K_{21} & \Delta K_{22} & \Delta K_{23} \\ \Delta K_{31} & \Delta K_{32} & \Delta K_{33} \end{bmatrix}, \tag{19}$$

for $2j\frac{\pi}{n}<\psi<(2j+1)\frac{\pi}{n}$, $j=0,1,2,\ldots,n-1$

and

$$[\Delta M]=[\Delta C]=[\Delta K]=[0], \tag{20}$$

for $(2j+1)\frac{\pi}{n}\le\psi\le(2j+2)\frac{\pi}{n}$, $j=0,1,2,\ldots,n-1$.

The elements of $[\Delta C]$ and $[\Delta K]$ are given, respectively, by:

$$\begin{aligned}
\Delta C_{11} &= 2\overline{m}_{ss}\sum_{k=1}^{N}\left(F_{ssbj}-F_{sjbi}\right)V_{0k} \\
\Delta C_{12} &= -2\overline{m}_{ss}(\beta_{pc}\delta_{sj1}+\sum_{k=1}^{N}F_{sjbi}W_{0k}) \\
\Delta C_{13} &= \Delta C_{22}=\Delta C_{23}=\Delta C_{31}=\Delta C_{32}=\Delta C_{33}=0 \\
\Delta C_{21} &= 2\overline{m}_{ss}(\beta_{pc}\delta_{sj1}+\sum_{k=1}^{N}F_{ssbj}W_{0k})
\end{aligned} \tag{21}$$

and

$$\begin{aligned}
\Delta K_{11} &= \left[\Lambda_{2ss}-(\Lambda_{2ss}-\Lambda_{1ss})\sin^2(\Re\theta)\right]\Delta_{sj1}+\overline{m}_{ss}(D_{sj}-\delta_{sj1}) \\
&\quad -(\Lambda_{2ss}-\Lambda_{1ss})\sum_{k=1}^{N}K_{sbjk}\phi_{0k}\sin(2\Re\theta) \\
\Delta K_{12} &= (\Lambda_{2ss}-\Lambda_{1ss})\frac{\sin(2\Re\theta)}{2}\Delta_{sj1} \\
&\quad +(\Lambda_{2ss}-\Lambda_{1ss})\sum_{k=1}^{N}K_{sbjk}\phi_{0k}\cos(2\Re\theta) \\
\Delta K_{13} &= (\Lambda_{2ss}-\Lambda_{1ss})\sum_{k=1}^{N}K_{sjbk}[W_{0k}\cos(2\Re\theta)-V_{0k}\sin(2\Re\theta)] \\
\Delta K_{21} &= (\Lambda_{2ss}-\Lambda_{1ss})\frac{\sin(2\Re\theta)}{2}\Delta_{sj1} \\
&\quad +(\Lambda_{2ss}-\Lambda_{1ss})\sum_{k=1}^{N}K_{sbjk}\phi_{0k}\cos(2\Re\theta) \\
\Delta K_{22} &= \overline{m}_{ss}D_{sj}+\left[\Lambda_{1ss}+(\Lambda_{2ss}-\Lambda_{1ss})\sin^2(\Re\theta)\right]\Delta_{sj1} \\
&\quad +(\Lambda_{2ss}-\Lambda_{1ss})\sum_{k=1}^{N}K_{sbjk}\phi_{0k}\sin(2\Re\theta) \\
\Delta K_{23} &= (\Lambda_{2ss}-\Lambda_{1ss})\sum_{k=1}^{N}K_{sjbk}[V_{0k}\cos(2\Re\theta)+W_{0k}\sin(2\Re\theta)] \\
\Delta K_{31} &= (\Lambda_{2ss}-\Lambda_{1ss})\sum_{k=1}^{N}K_{ssjk}[W_{0k}\cos(2\Re\theta)-V_{0k}\sin(2\Re\theta)] \\
\Delta K_{32} &= (\Lambda_{2ss}-\Lambda_{1ss})\sum_{k=1}^{N}K_{ssjk}[V_{0k}\cos(2\Re\theta)+W_{0k}\sin(2\Re\theta)] \\
\Delta K_{33} &= \mu_{ss}^{\ 2}K_{ss}N_{sj}+\kappa_{ss}\Delta_{sj2}+\left(\mu_{2ss}^{\ 2}-\mu_{1ss}^{\ 2}\right)\cos(2\theta)\delta_{sj2}
\end{aligned} \tag{22}$$

where the non-dimensional beam properties and the integrals of the products of the basis functions found in $[\Delta M]$, $[\Delta C]$ and $[\Delta K]$ are :

$$\begin{aligned}
K_{ss} &= \frac{k_{Ass}^{\ 2}}{k_{ss}^{\ 2}} & \mu_{1ss} &= \frac{k_{m1ss}}{R} \\
\mu_{2ss} &= \frac{k_{m2ss}}{R} & \mu_{ss} &= \frac{k_{mss}}{R} \\
\overline{m}_{ss} &= \frac{m_{ss}}{m} & \Lambda_{1ss} &= \frac{(EI)_{y'ss}}{m\Omega^2R^4} \\
\Lambda_{2ss} &= \frac{(EI)_{z'ss}}{m\Omega^2R^4} & \kappa_{ss} &= \frac{(GJ)_{ss}}{m\Omega^2R^4} \\
\delta_{sj1} &= \int_{\eta_1}^{\eta_2}\Psi_s\Psi_j\,d\bar{x} & \delta_{sj2} &= \int_{\eta_1}^{\eta_2}\Theta_s\Theta_j\,d\bar{x} \\
\Delta_{sj1} &= \int_{\eta_1}^{\eta_2}\Psi_s''\Psi_j''\,d\bar{x} & \Delta_{sj2} &= \int_{\eta_1}^{\eta_2}\Theta_s'\Theta_j'\,d\bar{x} \\
D_{sj} &= \int_{\eta_1}^{\eta_2}\frac{1-\bar{x}^2}{2}\Psi_s'\Psi_j'\,d\bar{x} & N_{sj} &= \int_{\eta_1}^{\eta_2}\frac{1-\bar{x}^2}{2}\Theta_s'\Theta_j'\,d\bar{x} \\
K_{sjk} &= \int_{\eta_1}^{\eta_2}\Theta_s\Psi_j''\Psi_k''\,d\bar{x} & F_{sjk} &= -\frac{1}{\beta_k^{\ 4}}\int_{\eta_1}^{\eta_2}\Psi_s'\Psi_j'\Psi_k''''\,d\bar{x}
\end{aligned} \tag{23}$$

The perturbation of this harmonic excitation is defined by a set of linear periodic differential equations:

$$\begin{Bmatrix} \tilde{\tilde{X}} \\ \tilde{\dot{X}} \\ \tilde{X} \end{Bmatrix}=[P(\psi)]\begin{Bmatrix} \tilde{\dot{X}} \\ \tilde{\ddot{X}} \\ \tilde{X} \end{Bmatrix} \tag{24.a}$$

with the solution

$$\begin{Bmatrix} \tilde{X}(T) \\ \tilde{\dot{X}}(T) \end{Bmatrix}=[Q(0,T)]\begin{Bmatrix} \tilde{X}(0) \\ \tilde{\dot{X}}(0) \end{Bmatrix} \tag{24.b}$$

Floquet's method for periodic systems was used in the present study to perform the stability analysis (Ref. 11). The eigenvalues of the transition matrix $Q(0,T)$ over one complete period of actuation, from $\psi=0$ to $\psi=T=2\pi/n$ were examined:

$$\begin{aligned}
\bar{\xi}_k &= (1/2T)\ln\left[\mathrm{Re}^2(\lambda_k)+\mathrm{Im}(\lambda_k)\right] \\
\bar{\omega}_k &= (1/T)\tan^{-1}\left[\mathrm{Im}(\lambda_k)/\mathrm{Re}(\lambda_k)\right]
\end{aligned} \tag{25}$$

The real part of the k^{th} eigenvalue of the transition matrix represents the non-dimensional growth/decay rate of the aeroelastic response to the system. A positive value indicates instability. The imaginary part of the same eigenvalue is associated with the non-dimensional frequency. Since the function $\tan^{-1}$ is multi-valued, the latter can be obtained only as a principal frequency plus or minus an integer multiple of $2\pi/T$.

3.2. "Smart" Blade Configuration

In order to present a realistic study case, a reduced scale model of a helicopter blade is developed. The model, resembling the EUROCOPTER BO105 helicopter blade, consists of a uniform main structure, made of Graphite-Epoxy composite, covered with a skin to form an airfoil cross section. The "smart" spring device is built into the blade by inserting "smart" materials i.e. piezoelectric materials, at any desired locations along the blade span.

The actuation of the "smart" spring increases the lead-lag, flap, torsional stiffness, and radii of gyration of the blade over a certain section of its length, i.e., along the location of the "smart" spring. In other words, the activation of the "smart" spring increases the impedance of the blade against the loads. The use of the "smart" spring as an IBC device is achieved by harmonically actuating the spring using a square wave (on-off) control law at various frequencies. Depending on its location and the length of the "smart" spring, the stability characteristics of the system will vary. Two design cases were considered in the present study. For the first case the "smart" spring is installed between 0.05 to 0.2, and for the second case between 0.05 to 0.40 in the normalized direction of the blade. The values of various configuration parameters related to the "smart" blade are tabulated in Table 1.

4.0. Numerical Results

The stability analysis of the hingeless "smart" blade was carried out by determining and comparing the eigenvalues of the controlled blade vs. the uncontrolled rotor. Certain parameters were chosen as the basis for an aeroelastic parametric study of instability in this investigation. These parameters are:

1. The span-wise location and the length of the "smart" spring, i.e. the starting and ending position of the "smart" spring, x_1 and x_2.
2. The flap-lag structural coupling, $\Re$.
3. The collective pitch angle, θ.

By varying the values of the parameters above, different system responses are obtained for the 1st lead-lag, 1st and 2nd flap, and 1st torsion modes and the aeroelastic stability of the system is thus analyzed. The parameters of the rotor model analyzed are also listed in Table 1.

Table 1: Rotor Model Analyzed

Parameter	Value
a	2π rad^{-1}
B	4
c	0.121 m
c_{d_0}	0.01
$EI_y/m\Omega^2R^4$	0.0017 (1)
$EI_z/m\Omega^2R^4$	0.0222 (2)
$GJ/m\Omega^2R^4$	0.001 (3)
R	2.0 m
$\Re$	1
β_{pc}	0°
γ	5.0
σ	0.077
Ω	110 rad/sec

(1) Corresponding to a normalized lead-lag frequency 0.7/rev at 110 rad/sec.
(2) Corresponding to a normalized first flap bending frequency 1.14/rev at 110 rad/sec.
(3) Corresponding to a normalized torsion frequency 3.9/rev at 110 rad/sec.

Another important aspect that must be noted in the stability analysis of the hingeless "smart" blade is the activation regime of the "smart" spring that results in various systems as outlined below:

1. **Baseline Regime:**
   The system consisting of only the main structure without any "smart" spring.
2. **Static Regime:**
   The system consisting of the main structure and the "smart" springs that is activated all the time.
3. **IBC 3 Regime:**
   The system consisting of the main structure and the "smart" spring that is activated and deactivated 3 times per rotor revolution.
4. **IBC 4 Regime:**
   The system consisting of the main structure and the "smart" spring that is activated and deactivated 4 times per rotor revolution.
5. **IBC 5 Regime:**
   The system consisting of the main structure and the "smart" spring that is activated and deactivated 5 times per rotor revolution.

For the Baseline and Static regimes the equations of motion have constant coefficients. Hence, for the Baseline, i.e., in the absence of any "smart' springs, the system's perturbation is defined by equations (14). For the Static Regime, i.e., continuously activated spring, the perturbations

of the system are defined by equations (16) where [M]+[ΔM], [C]+[ΔC], and [K]+[ΔK] are constants for all time t. In both cases, the corresponding eigenvalues can be determined using the conventional eigenvalue-eigenvector technique. On the contrary, since IBC 3, 4, and 5 are periodic systems then the eigenvalues are determined using Floquet method as outlined earlier.

4.1. Design Case 1: $x_1 = 0.05$, $x_2 = 0.20$, $\Re = 1.0$, $\theta = 0$ to 0.3

1st lead-lag mode: Table 2.1 shows the eigenvalues corresponding to the 1st lead-lag mode of the hingeless "smart" blade. As the pitch angle is increased from 0 to 0.3, an increase of damping are observed for all systems, i.e., Baseline, Static and IBC 3,4, and 5 regimes. The oscillation frequency decreases to zero at 0.3 pitch angle for the Baseline, Static, and IBC 3 and IBC 4 cases. Divergence is experienced at 0.3 pitch angle by the Baseline and Static regimes as each has one root on the real axis at the right-half- plane of the Laplace domain. At pitch angles greater than 0.3, IBC 4 becomes prone to divergence as one of its roots on the real axis is approaching the stability boundary. Thus, the presence of the "smart" spring being activated at 3, 4, and 5/rev indeed stabilize the hingeless blade.

Table 2.1. Eigenvalues of the "smart" blade for the 1st lead-lag mode with $x_1 = 0.05$, $x_2 = 0.2$, $\beta_{pc} = 0$, $\Re = 1.0$

θ (rad)	Baseline	Static	IBC 3	IBC 4	IBC 5
0.0	-0.001 +0.656*i*	-0.001 +0.775*i*	-0.001 +0.718*i*	-0.001 +0.718*i*	-0.001 +0.718*i*
0.1	-0.057 +0.6052*i*	-0.047 +0.766*i*	-0.018 +0.668*i*	-0.020 +0.664*i*	-0.020 +0.658*i*
0.2	-0.158 +0.422*i*	-0.197 +0.696*i*	-0.191 +0.586*i*	-0.186 +0.583*i*	-0.205 +0.569*i*
0.3	0.456; -1.411	0.319; -1.471	-0.082; -1.091	-0.001 ; -1.144	-0.340 +0.205*i*

1st flap mode: All systems experience decreasing damping for the 1st flap mode when the pitch angle is increased from 0 to 0.3 as can be seen in Table 2.2. A sharp decrease in damping of the Static and IBC 5 regimes make them sensitive to flutter if the pitch angle is increased beyond 0.3.

Table 2.2. Eigenvalues of the "smart" blade for the 1st flap mode with $x_1 = 0.05$, $x_2 = 0.2$, $\beta_{pc} = 0$, $\Re = 1.0$

θ (rad)	Baseline	Static	IBC 3	IBC 4	IBC 5
0.0	-0.324 +0.971*i*	-0.329 +1.07*i*	-0.326 +0.476*i*	-0.339 +0.971*i*	-0.334 +0.481*i*
0.1	-0.269 +0.958*i*	-0.274 +1.05*i*	-0.338 +0.477*i*	-0.309 +0.958*i*	-0.353 +1.069*i*
0.2	-0.175 +0.989*i*	-0.130 +1.05*i*	-0.144 +0.482*i*	-0.138 +0.983*i*	-0.133 +1.013*i*
0.3	-0.095 +0.926*i*	-0.037 +0.926*i*	-0.184 +0.174*i*	-0.247 +0.853*i*	-0.037 +1.011*i*

2nd flap mode: A similar trend as the 1st flap mode is observed in the 2nd flap mode as can be seen in Table 2.3. As the pitch angle is increased from 0 to 0.3, all systems experience a decrease in damping, i.e., moving towards the unstable region. A very rapid decrease of damping is observed for both IBC 3 and IBC 4 when the pitch angle is increased from 0.2 to 0.3. If the pitch angle was increased beyond 0.3, both IBC 3 and IBC 4 will have experienced flutter.

Table 2.3. Eigenvalues of the "smart" blade for the 2nd flap mode with $x_1 = 0.05$, $x_2 = 0.2$, $\beta_{pc} = 0$, $\Re = 1.0$

θ (rad)	Baseline	Static	IBC 3	IBC 4	IBC 5
0.0	-0.758 +1.908*i*	-0.816 +1.977*i*	-0.785 +3.443*i*	-0.786 +4.045*i*	-0.787 +5.555*i*
0.1	-0.720 +1.885*i*	-0.787 +1.967*i*	-0.728 +3.400*i*	-0.743 +4.091*i*	-0.747 +4.596*i*
0.2	-0.681 +1.724*i*	-0.754 +1.817*i*	-0.708 +3.270*i*	-0.711 +4.224*i*	-0.712 +5.727*i*
0.3	-0.434 +1.156*i*	-0.440 +1.336*i*	-0.173 +3.650*i*	-0.108 +4.911*i*	-0.501 +5.957*i*

1st torsion mode: Table 2.4 shows an increase of damping for the 1st torsion mode of all systems as the pitch angle is increased from 0 to 0.3. At 0.3 pitch angle, all the systems are highly damped and thus the amplitude of response will quickly decrease. A particularly interesting situation is observed for IBC 3

Regime where the system responds in a damped, non-oscillatory manner at 0 pitch, while its damping increases as the pitch angle increases. A negative pitch angle on IBC 3 Regime might result in divergence due to the separation of the roots on the real axis of the Laplace domain.

Table 2.4. Eigenvalues of the "smart" blade for the 1st torsion mode with $x_1 = 0.05$, $x_2 = 0.2$, $\beta_{pc} = 0$, $\Re = 1.0$

θ (rad)	Baseline	Static	IBC 3	IBC 4	IBC 5
0.0	-0.304 +2.761*i*	-0.362 +3.234*i*	-0.318; -0.352	-0.322 +4.997*i*	-0.325 +6.023*i*
0.1	-0.386 +3.018*i*	-0.619 +4.095*i*	-0.494 +3.592*i*	-0.507 +4.425*i*	-0.459 +6.067*i*
0.2	-0.536 +3.543*i*	-1.065 +4.902*i*	-0.804 +3.265*i*	-0.813 +4.198*i*	-0.799 +5.788*i*
0.3	-0.784 +4.009*i*	-1.024 +4.709*i*	-0.990 +3.157*i*	-1.007 +4.565*i*	-1.055 +5.444*i*

4.2. Design Case 2: $x_1 = 0.05$, $x_2 = 0.40$, $\Re = 1.0$, $\theta = 0$ to 0.3

1st lead-lag mode: Table 3.1 shows the eigenvalues corresponding to the 1st lead-lag mode of the hingeless "smart" blade where trends similar to Design Case 1 are observed. As the pitch angle is increased from 0 to 0.3, an increase of damping are observed for all systems, i.e., Baseline, Static and IBC 3, 4, 5 regimes. For all systems, the oscillation frequency decreases to zero at 0.3 pitch angle and separation of roots on the real axis takes place. As the result, divergence is experienced at 0.3 pitch angle by Baseline, IBC 3, 4 and 5 regimes as each has one root on the real axis at the right-half-plane of the Laplace domain. The Static Regime, however, is damped without oscillation and becomes prone to divergence as one of its roots on the real axis is approaching the stability boundary at 0.3 pitch angle. At this condition, with the activation of "smart" spring, the blade still experiences divergence.

Table 3.1. Eigenvalues of the "smart" blade for the 1st lead-lag mode with $x_1 = 0.05$, $x_2 = 0.4$, $\beta_{pc} = 0$, $\Re = 1$

θ (rad)	Baseline	Static	IBC 3	IBC 4	IBC 5
0.0	-0.001 +0.656*i*	-0.001 +0.996*i*	-0.001 +0.650*i*	-0.001 +0.846*i*	-0.001 +0.845*i*
0.1	-0.057 +0.605*i*	-0.034 +1.010*i*	-0.046 +0.651*i*	-0.035 +0.848*i*	-0.045 +0.847*i*
0.2	-0.158 +0.422*i*	-0.258 +0.959*i*	-0.368 +0.208*i*	-0.310 +0.796*i*	-0.352 +0.817*i*
0.3	-1.411; 0.456	-0.282; -0.914	-1.263; 0.336	-0.638; 0.370	-1.349; 0.298

1st flap mode: For the 1st flap mode, all systems experience a rapid decrease in damping towards the stability boundary when the pitch angle is increased from 0 to 0.3 as can be seen in Table 3.2. Flutter occurs for the Static Regime at 0.3 pitch angle while IBC 3 and 4 are sensitive to flutter if the pitch angle is increased beyond 0.3.

Table 3.2. Eigenvalues of the "smart" blade for the 1st flap mode with $x_1 = 0.05$, $x_2 = 0.4$, $\beta_{pc} = 0$, $\Re = 1$

θ (rad)	Baseline	Static	IBC 3	IBC 4	IBC 5
0.0	-0.324 +0.971*i*	-0.337 +1.206*i*	-0.331 +0.403*i*	-0.348 +0.917*i*	-0.336 +1.094*i*
0.1	-0.269 +0.958*i*	-0.303 +1.177*i*	-0.304 +0.424*i*	-0.336 +0.903*i*	-0.330 +1.045*i*
0.2	-0.175 +0.989*i*	-0.073 +1.190*i*	-0.077 +0.694*i*	-0.068 +0.677*i*	-0.063 +0.673*i*
0.3	-0.096 +0.926*i*	0.061 +1.243*i*	-0.041 +0.089*i*	-0.010 +0.736*i*	-0.072 +1.139*i*

2nd flap mode: The Baseline and Static regimes start with a high damping and a non-zero oscillation frequency at 0 pitch angle and continue with a decrease in both the damping and oscillation frequency for the 2nd flap mode, Table 3.3. An interesting behaviour is exhibited by IBC 3 and IBC 5. A decrease in damping occurs in the systems when the pitch angle is increased from 0 to 0.2. This is followed by a reversed effect of increasing damping as the pitch angle is increased from 0.2 to 0.3. Thus, for this mode in all IBC systems, the decay rate of the response is increased at higher pitch

angles rather than promoting unstable response, which is a desirable output. IBC 4 is damped without oscillation at lower pitch angles of 0 to 0.1 and as the pitch angle increases, its response follows the same trends described above.

Table 3.3. Eigenvalues of the "smart" blade for the 2nd flap mode with $x_1 = 0.05$, $x_2 = 0.4$, $\beta_{pc} = 0$, $\Re = 1$

θ (rad)	Baseline	Static	IBC 3	IBC 4	IBC 5
0.0	-0.758 +1.908*i*	-0.908 +2.127*i*	-0.846 +3.495*i*	-0.931; -0.766	-0.838 +5.478*i*
0.1	-0.720 +1.885*i*	-0.887 +2.108*i*	-0.840 +3.429*i*	-0.906; -0.786	-0.817 +5.500*i*
0.2	-0.682 +1.724*i*	-0.848 +1.959*i*	-0.673 +3.312*i*	-0.712 +4.225*i*	-0.715 +5.722*i*
0.3	-0.434 +1.156*i*	-0.521 +1.215*i*	-0.831 +3.385*i*	-1.052 +4.532*i*	-0.951 +6.150*i*

1st torsion mode: Table 3.4 shows an increase of damping and oscillation frequency for the 1st torsion mode of the Baseline and Static regimes as the pitch angle is increased from 0 to 0.3. At 0.3 pitch angle, the Baseline Regime becomes highly damped and thus the amplitude of response will quickly decrease. Just like the corresponding system in Design Case 1, IBC 3 presents a particularly interesting situation. As the pitch angle is increased from 0 to 0.1, the oscillation frequency drops to reach zero at 0.1 pitch angle, which results in a damped, non-oscillatory response. As the pitch angle varies from 0.1 to 0.3, damping and frequency increase to non-zero values. IBC 4 responds with an increasing damping as the pitch angle varies from 0 to 0.3. IBC 5 also responds in an interesting manner in which the damping increases as the pitch angle is increased from 0 to 0.2. This is followed by a sharp decline in damping as the pitch angle is further increased to 0.3 thus making the system prone to flutter at higher pitch angle.

Table 3.4. Eigenvalues of the "smart" blade for the 1st torsion mode with $x_1 = 0.05$, $x_2 = 0.4$, $\beta_{pc} = 0$, $\Re = 1$

θ (rad)	Baseline	Static	IBC 3	IBC 4	IBC 5
0.0	-0.304 +2.761*i*	-0.184 +2.768*i*	-0.231 +3.213*i*	-0.211 +4.779*i*	-0.233 +5.300*i*
0.1	-0.386 +3.018*i*	-0.217 +2.849*i*	-0.282; -0.211	-0.219 +4.852*i*	-0.245 +5.541*i*
0.2	-0.536 +3.543*i*	-0.266 +3.023*i*	-0.380 +3.304*i*	-0.408 +4.716*i*	-0.368 +6.245*i*
0.3	-0.784 +4.009*i*	-0.453 +3.586*i*	-0.315 +3.591*i*	-0.455 +4.962*i*	-0.102 +6.173*i*

5.0. Conclusions

In general, the results of the analysis indicate that harmonic parametric actuation of the "smart" spring affects the aeroelastic stability of the hingeless helicopter blade. Some unstable conditions encountered in the Basic hingeless blade at high pitch angles can be stabilized using IBC. However, due to the complex manner in which various parameters such as the length/ position of the "smart" spring, the pitch angle of the rotor, or the frequency of the harmonic actuation of the "smart" spring, affect the behaviour of the rotor, one may expect that IBC will not always be beneficial to the overall stability of the system. As noted by Bolotin (Ref. 12), stability problems may arise when the harmonic parametric excitation approaches the frequency associated with the structural modes. The present study also reveals that the aeroelastic behaviour of the system changes significantly with the presence of the "smart" spring. Thus, a carefully engineered "smart" spring technology, applied on a hingeless helicopter rotor blade, may improve the quality of the helicopter operation.

The Stability of the 1st Lead-Lag Mode: One important finding about the harmonically actuated "smart" blade that was considered is that it improves the general stability of the 1st lead-lag mode response of the Baseline system for both design cases considered. The application of the IBC concept using the "smart" spring technology at 3, 4, and 5 actuations per blade revolution result in the aeroelastic stability for Design Case 1 when the Baseline system experiences divergence at a high pitch angle of

0.3 radians (17 degrees). For Design Case 2, however, at 0.3 pitch angle, the IBC fails to stabilize the system at all regimes.

The Stability of the 1st Flap Mode: For Design Case 1, IBC 3 and 4 are beneficial in terms of improving the stability of the Baseline system at 0.3 pitch angle for the 1st flap mode, i.e., both IBC regimes increase damping of the rotor. On the other hand, under the same operation, all IBC regimes in Design Case 2 result in lower damping than that of the Baseline system.

The Stability of the 2nd Flap Mode: The 2nd flap mode presents an interesting study case where, depending on the length of the "smart" spring and the frequency of its harmonic actuation, the application of the IBC concept can be either favourable or unfavourable towards improving the stability of the blade. As one can observe in Design Case 2, the IBC systems significantly improve the stability of the Baseline system at high pitch angles by increasing the damping as θ varies from 0.2 to 0.3. For Design Case 1, the harmonic actuation of the "smart" spring at IBC 3 and IBC 4 result in a sharp drop in damping between 0.2 to 0.3 pitch angle, while IBC 5 results in improved stability at 0.3 pitch angle.

The Stability of the 1st Torsion Mode: In general, it is observed that for this mode damping increases as the pitch angle is increased. For Design Case 2, IBC 5 initially increases the damping up to 0.2 pitch angle. This is followed by a sharp drop in damping towards the stability boundary at 0.3 pitch angle. This indicates that for this design, i.e., the "smart" spring located between 5% to 40% in the axial direction, its actuation at 5/rev will result in undesirable conditions of stability for the 1st torsion mode at pitch angles greater or equal to 0.3.

The evaluation of the behaviour of the harmonic actuation of the "smart" spring also reveals that under certain conditions, IBC results in damped, non-oscillatory response. In these regions, the eigenvalues of the system lie on the real axis of the Laplace domain, i.e., at the zero frequency line with relatively high damping. For the 2nd flap mode, in Design Case 2, the IBC 4 behaves in such a way at low pitch angles. For each design case, IBC 3 can result in a damped, non- oscillatory response for the 1st torsion mode at certain values of pitch angle.

Considering the improvement in the 1st lead-lag stability of the Baseline Regime for Design Case 1 in terms of increasing modal damping at 0.3 pitch angle, one may suggest the application of "smart" spring to control aeromechanical phenomena such as ground and air resonance.

References

1. Kretz, M., "Research in Multicyclic and Active Control of Rotary Wings," Vertica, Vol.1, No 1 / 2, 1976, pp. 95-105.

2. Ham, N.D., "Helicopter Individual Blade Control at MIT 1977-1985", Vertica, Vol. 11, No. 1 / 2, 1987, pp. 109-122.

3. Spangler, R.L., Jr. and Hall, S. R., "Piezoelectric Actuators for Helicopter Rotors Control', Proceedings: AIAA/ASME/ASCE/AHS/ASC 31. Structures, Structural Dynamics and Materials Conference, AIAA, Washington, DC, 1990, Part 3, pp.1589-1599.

4. Nitzsche, F., Lammering, R., Breitbach, E., "Can Smart Materials Modify Blade Root Boundary Conditions to Attenuate Helicopter Vibration?" in Fourth International Conference on Adaptive Structures, E.J. Breitbach, B.K. Wada and M. C. Natori editors, Technomic, Lancaster-Basel, 1994, pp. 139-150.

5. Nitzsche, F.; "Modelling an Adaptive Impedance Boundary Condition Device for Helicopter Individual Blade Control"; Smart Structures Materials; SPIE Vol. 3039: Proceedings; 1997; pages: 216-226.

6. Hodges, D.H.; Dowell, E.H.; "Non-Linear Equations of Motion for the Elastic Bending and Torsion of Twisted Nonuniform Rotor Blades"; NASA TN D-7818; December 1974.

7. Hodges, D.H.; Ormiston, R.A. ; "Stability of Elastic Bending and Torsion of Uniform Cantilever Rotor Blade in Hover with variable Structural Coupling"; NASA TN D-8192; April 1976.

8. Greenberg, J.M; "Airfoil in Sinusoidal Motion in Pulsating Stream"; NACA TN 1326; 1947.

9. Chang, T.C.; Craig, R. R. Jr.; "On Normal Modes of Uniform Beams; ERML. 1068; University of Texas (Austin); 1969.

10. Solaiman, S. and Afagh, F.F.; "Helicopter Individual Blade Control Strategies using "Smart" Structures" Final Report; PWSGC Contract No. 31184-6-0296/001/ST; Carleton University, Ottawa, Canada; June 1999.

11. Dugundji, J.; Wendell, J.H.; "Some Analysis Methods for Rotating Systems with Periodic Coefficients"; AIAA Journal; Vol. 21; no. 6;1982.

12. Bolotin, V.V.; "Dynamic Stability of Elastic Systems"; Holden-Day Inc., 1964.